

# ANOMALY DETECTION BASED QUENCH DETECTION SYSTEM FOR CW OPERATION OF SRF CAVITIES\*

G. Martino<sup>†1,4</sup>, A. Bellandi<sup>1</sup>, A. Eichler<sup>1</sup>, J. Branlard<sup>1</sup>, H. Schlarb<sup>1</sup>, L. Doolittle<sup>2</sup>, S. Aderhold<sup>3</sup>, S. Hoobler<sup>3</sup>, J. Nelson<sup>3</sup>, R. D. Porter<sup>3</sup>, L. Zacarias<sup>3</sup>, A. Benwell<sup>3</sup>, D. Gonnella<sup>3</sup>, A. Ratti<sup>3</sup>, and G. Fey<sup>4</sup>

<sup>1</sup>DESY, 22607 Hamburg, Germany

<sup>2</sup>LBNL, 94720 Berkley, CA, USA

<sup>3</sup>SLAC, 94025 Menlo Park, CA, USA

<sup>4</sup>TUHH, 21073 Hamburg, Germany

## Abstract

Superconducting radio frequency (SRF) cavities are used in modern particle accelerators to take advantage of their very high quality factor (Q). A higher Q means that a higher RF field can be sustained, and a higher acceleration can be produced in the cavity for length unity. However, in certain situations, e.g., too high RF field, the SRF cavities can experience quenches that risk creating damage due to the rapid increase in the heat load. This is especially negative in continuous wave (CW) operation due to the impossibility of the system to recover during the off-load period. The design goal of a quench-detection system is to protect the system without being a limiting factor during the operation. In this paper, we compare two different classification approaches for improving a quench detection system. We perform tests using traces recorded from LCLS-II and show that the AR-SENAL classifier outperforms a CNN classifier in terms of accuracy.

## INTRODUCTION

Modern linear accelerators use superconducting radio frequency (SRF) cavities as the main component for achieving high accelerating gradients. SRF cavities are used due to their superior energy efficiency for the same accelerating gradient and lower beam impedance. This means reaching higher particle energies than normally possible at a lower operating cost [1]. However, a lot of care needs to be posed to the control system of SRF cavities due to the high susceptibility to external factors, e.g., external microphonics and Lorentz force detuning [2]. One of the main limiting factors for SRF cavities is the disruption of the superconductivity in part or the entirety of the cavity. Such superconductivity disruption is also referred to as quench. Quenches are mainly caused by defects or contamination of the material [3]. They must be avoided since the disruption of the superconductivity leads to an increased heat load and subsequent lengthy disruptions in the cryogenic system.

The detection of quenches is usually performed by estimating the value of the unloaded quality factor  $Q_0$ . However,

we can only measure the loaded quality factor  $Q_L$ , which relates to  $Q_0$  and the external quality factor  $Q_{ext}$  as follows:

$$\frac{1}{Q_L} = \frac{1}{Q_{ext}} + \frac{1}{Q_0} \quad (1)$$

Typical values for  $Q_{ext}$  and  $Q_0$  in normal conditions are approximately  $3 \times 10^6$  and  $2 \times 10^{10}$ , respectively. In the case of a quench,  $Q_0$  can reach values as low as  $10^7$ . With such values, from Eq. 1, it can be derived that it is necessary to detect minimal variations of the value of  $Q_L$ .

The decrease of  $Q_L$ , e.g., as a result of a quench, can be detected as an increase of the cavity half bandwidth  $f_{(1/2)}$ . In pulsed machines, the amplitude decay estimation can be used to calculate  $f_{(1/2)}$  thanks to the following:

$$f_{(1/2)} = \frac{f_0}{2Q_L} = \frac{1}{2\pi\tau} \quad (2)$$

where  $f_0$  is the cavity resonance frequency and  $\tau$  is the exponential time constant of the cavity gradient decay. In CW machines, since no amplitude decay is available during normal operation, it is necessary to use the cavity signals expressed as in-phase and quadrature ( $I&Q$ ) components. For the half bandwidth calculation, starting from the cavity dynamics model, the following is used:

$$f_{(1/2)} = \frac{I_p \left( KI_f + BI_B - \frac{\dot{I}_p}{2\pi} \right) + Q_p \left( KQ_f + BQ_B - \frac{\dot{Q}_p}{2\pi} \right)}{I_p^2 + Q_p^2} \quad (3)$$

where  $K = \frac{f_0}{Q_{ext}}$ ,  $B = \frac{f_0}{2} r/Q$ ,  $r/Q$  is the geometric shunt impedance, and the subscripts  $p$ ,  $f$  and  $b$  refer to the probe, forward, and beam current signals, respectively. A possible different approach for the detection of a quench can be derived from the estimation of the cavity power dissipation:

$$P_{diss} = P_f - P_r - \dot{U} \quad (4)$$

where  $P_f$  is the forward power,  $P_r$  is the reflected power, and  $U = \frac{V^2}{f_0(r/Q)}$  is the cavity stored energy equation. In this case, an increase in the cavity power dissipation above a certain threshold indicates a cavity quench.

The approaches presented for CW machines require a precise calibration of the cavity signals and suffer noisy signals.

\* This work is supported by DASHH (Data Science in Hamburg — HELMHOLTZ Graduate School for the Structure of Matter) under Grant No.: HIDSS-0002.

† gianluca.martino@desy.de

Content from this work may be used under the terms of the CC BY 4.0 licence (© 2021). Any distribution of this work must maintain attribution to the author(s), title of the work, publisher, and DOI

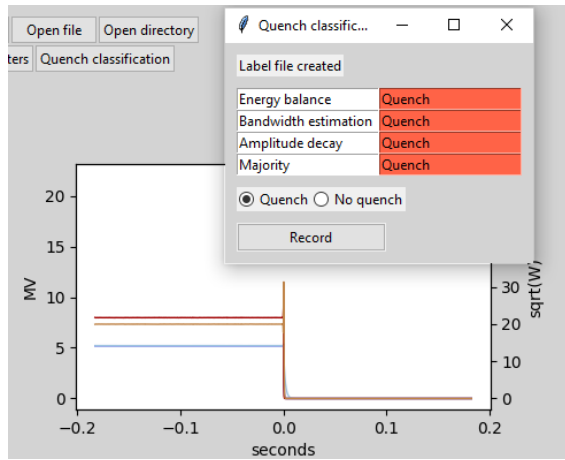


Figure 1: Fault display classification window.

For those reasons, it is possible to have false quenches with a consequent trip that results in unnecessary downtime.

In this paper, we compare two different approaches for supervised anomaly detection in time series: 1) a Convolutional Neural Network (CNN) classifier based on the work in [4]; 2) an ensemble of ROCKET classifiers [5].

The dataset used has been obtained during LCLS-II commissioning. LCLS-II is a superconducting linear accelerator (LINAC) at SLAC that results from the collaboration between multiple laboratories. LCLS-II operates in CW operation mode to accelerate an electron beam with a repetition rate of 1-MHz. Additionally, for this project, we built the LCLS-II fault display, a panel that helps identify, analyze and categorize faults. The main component is a user interface that enables the data selection for the training of the quench detection scheme. The user interface is composed of plot displays for the visualization of cavity signals and processed data, e.g., the calculation of the quench detection system.

## LCLS-II FAULT DISPLAY

The main goal of a fault analysis interface is to provide the means for performing incident review and post-mortem analysis. Specifically, it needs to provide a way to review past events, identify causes and debug.

The LCLS-II fault display allows for visualizing previous faults, automatically saved by the control system. Since the initial focus of this project was on the quench detection system, the fault display also calculates and plots the cavity power dissipation. The calculations are performed independently of the FPGA to exclude bugs in the implementation.

A quench classification panel has been added to introduce the human-in-the-loop paradigm. The goal of this panel is to aid the classification of the events. At this stage, the classification is relative only to quench events.

This quench classification panel gives an initial guess about whether or not the event is a quench based on all three methods explained. However, there are multiple ways for those methods to fail, e.g., uncalibrated signals or data

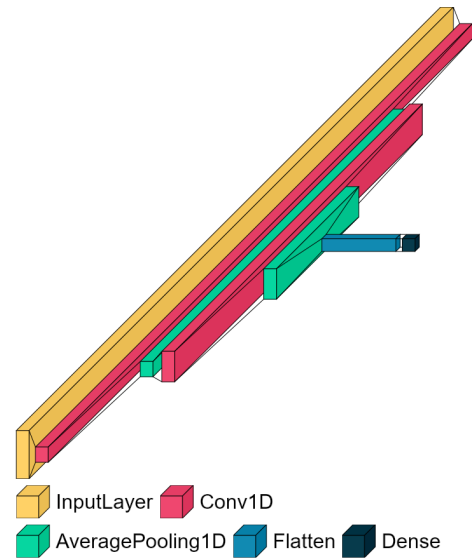


Figure 2: CNN network structure.

corruption. For this reason, the expert needs to manually select whether the event is a quench or not. A screenshot of the quench labeling interface is shown in Fig. 1.

## ROBUST QUENCH DETECTION

During normal machine operation, a quench detection system based on the cavity model can reach a false positive rate of up to 47%. For this reason, a more robust method for quench detection is an active research area [6, 7]. While classical methods use the cavity model to compute a signal that represents a residual, improved quench detection schemes require adding signals to add robustness to the classification.

We compare two methods for classification using the waveforms of the amplitude, phase, power, I, and Q signals from the cavity, the forward, and the reverse probes. Additionally, each data point is enhanced with additional waveforms, calculated starting from Formula 4. Specifically, we add the calculated cavity stored energy, the system stored energy, and the waveguide energy estimations.

The CNN classifier uses a sequence of convolutional layers interspersed with average pooling layers for filtering and down-sampling, respectively. The structure of the classifier is represented in Fig. 2. This CNN structure shows good classification accuracy with multivariate time series and good noise tolerance [4].

The ensemble classifier is composed of 5 ROCKET classifiers using a ridge classifier with built-in cross-validation [8] for the generation of the final classification.

## EXPERIMENTAL RESULTS

The dataset used contains all fault traces stored during LCLS-II commissioning. The data is stored when a trip occurs and is tagged with the system that triggered the trip event. Each data point contains multiple waveforms and is enhanced with additional waveforms, calculated starting

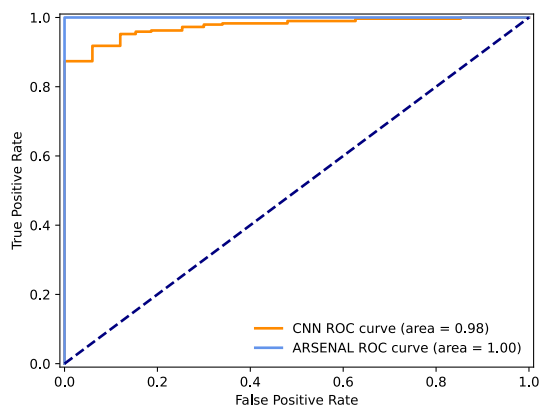


Figure 3: AUROC curves for the entire waveforms.

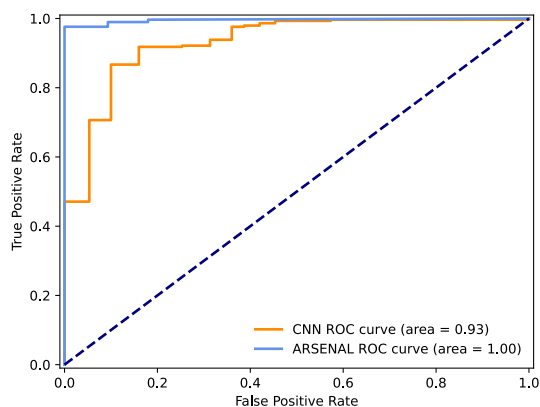


Figure 4: AUROC curves for the reduced waveforms.

from Formula 4. The waveforms stored start 2 ms before the event, end 2 ms after the event, and contain 2048 timepoints. The dataset is split equally between training and testing set. We performed two experiments:

- in the first experiment, the dataset includes the entire waveforms;
- in the second experiment, the waveforms are reduced to include all timepoints leading to the trip event but excluding the event itself and a variable number of timepoints preceding.

The results are evaluated by using the Receiver Operating Characteristic (ROC) curve. The AUROC score is defined as the area underneath the ROC curve and ranges between 0 and 1. An AUROC score of 1 represents a predictor whose predictions are 100% correct. An AUROC score of 0 represents a predictor whose predictions are 100% wrong, i.e., opposite predictions. Finally, an AUROC score of 0.5 represents a predictor whose predictions are random guesses.

In the first experiment, we test the detection capabilities of the algorithms. The result of the first experiment is shown in Figure 3. In the second experiment, we test the prediction capabilities of both algorithms instead. This is possible since the quench threshold is never surpassed in both datasets. The result of the second experiment is shown in Figure 4.

The results for both experiments show that the ARSENAL approach performs better both in prediction and detection. The accuracy scores recorded for the second experiment are 0.96 for the ARSENAL classifier and 0.86 for the CNN classifier.

## CONCLUSION AND OUTLOOK

The experiments show that it is feasible to predict whether the running conditions represented by a set of traces will lead to a quench before the value calculated based on the cavity model surpasses the quench threshold. However, utilizing such a technique in a real machine requires fast reaction and prediction times. The next step will be to implement both techniques in field programmable gate arrays (FPGAs) to reduce both computation time and latency of the calculations.

Additionally, we presented a fault display that allows performing post-mortem analysis and incident review for most quench-related faults and more. However, additional data representation will help further improve the analysis capabilities. A future addition will be the bit-accurate representation of the signals processed in FPGA, to be compared to a simulated version of the same traces. Such plots can help identify FPGA-related issues that are not visible otherwise.

## REFERENCES

- [1] P. Schmüser, “Basic principles of rf superconductivity and superconducting cavities,” 2006. doi:10.5170/CERN-2006-002.183
- [2] A. Bellandi *et al.*, “Online detuning computation and quench detection for superconducting resonators,” *IEEE Transactions on Nuclear Science*, vol. 68, no. 4, pp. 385–393, 2021. doi:10.1109/TNS.2021.3067598
- [3] M. S. Champion *et al.*, “Quench-limited srf cavities: Failure at the heat-affected zone,” *IEEE Transactions on Applied Superconductivity*, vol. 19, no. 3, pp. 1384–1386, 2009. doi:10.1109/TASC.2009.2019204
- [4] B. Zhao, H. Lu, S. Chen, J. Liu, and D. Wu, “Convolutional neural networks for time series classification,” *Journal of Systems Engineering and Electronics*, vol. 28, no. 1, pp. 162–169, 2017. doi:10.21629/JSEE.2017.01.18
- [5] A. Dempster, F. Petitjean, and G. I. Webb, “ROCKET: Exceptionally fast and accurate time series classification using random convolutional kernels,” *Data Mining and Knowledge Discovery*, vol. 34, no. 5, pp. 1454–1495, 2020. doi:10.1007/s10618-020-00701-z
- [6] A. Eichler, J. Branlard, and J. H. K. Timm, *Anomaly detection at the european xfel using a parity space based method*, 2022. doi:10.48550/ARXIV.2202.02051
- [7] A. Nawaz, S. Pfeiffer, G. Lichtenberg, and P. Rostalski, “Anomaly detection for the european xfel using a nonlinear parity space method,” *IFAC-PapersOnLine*, vol. 51, no. 24, pp. 1379–1386, 2018, 10th IFAC Symposium on Fault Detection, Supervision and Safety for Technical Processes SAFEPROCESS 2018. doi:10.1016/j.ifacol.2018.09.554
- [8] T. Hastie, R. Tibshirani, and J. Friedman, *The elements of statistical learning: data mining, inference and prediction*, 2nd ed. Springer, 2009.